

Intense white laser of high spectral flatness via optical-damage-free water–lithium niobate module

Lihong Hong,^{a,b} Yuanyuan Liu,^b Haiyao Yang,^b Lingzhi Peng,^b Mingzhou Li,^b Yujie Peng^{✉,a},
Ruxin Li,^a and Zhi-Yuan Li^{b,*}

^aChinese Academy of Sciences, Shanghai Institute of Optics and Fine Mechanics, State Key Laboratory of High Field Laser Physics, Shanghai, China

^bSouth China University of Technology, School of Physics and Optoelectronics, Guangzhou, China

Abstract. A supercontinuum white laser with ultrabroad bandwidth, intense pulse energy, and high spectral flatness can be accomplished via synergic action of third-order nonlinearity (3rd-NL) and second-order nonlinearity. In this work, we employ an intense Ti:sapphire femtosecond laser with a pulse duration of 50 fs and pulse energy up to 4 mJ to ignite the supercontinuum white laser. Remarkably, we use water instead of the usual solid materials as the 3rd-NL medium exhibiting both strong self-phase modulation and stimulated Raman scattering effect to create a supercontinuum laser with significantly broadened bandwidth and avoid laser damage and destruction. Then the supercontinuum laser is injected into a water-embedded chirped periodically poled lithium niobate crystal that enables broadband and high-efficiency second-harmonic generation. The output white laser has a 10 dB bandwidth encompassing 413 to 907 nm, more than one octave, and a pulse energy of 0.6 mJ. This methodology would open up an efficient route to creating a long-lived, high-stability, and inexpensive white laser with intense pulse energy, high spectral flatness, and ultrabroad bandwidth for application to various areas of basic science and high technology.

Keywords: intense white laser; optical-damage-free; water; third-order nonlinearity; second-order nonlinearity.

Received Oct. 24, 2023; revised manuscript received Nov. 29, 2023; accepted for publication Dec. 16, 2023; published online Jan. 12, 2024.

© The Authors. Published by SPIE and CLP under a Creative Commons Attribution 4.0 International License. Distribution or reproduction of this work in whole or in part requires full attribution of the original publication, including its DOI.

[DOI: [10.1117/1.APN.3.1.016008](https://doi.org/10.1117/1.APN.3.1.016008)]

1 Introduction

The drive to construct ultrabroadband laser light sources is fueled by a host of tantalizing applications, such as large-scale imaging of biological dynamics,¹ femtochemistry,² telecommunications,³ sensing, and ultrafast science.⁴ Many of these applications require developing a so-called three-high supercontinuum white laser with large pulse energy and high peak power, large spectral bandwidth, and a superflat spectral profile. For example, spectrally broad and flat light sources with high pulse energy are essential for simultaneously resolving multiple absorption bands and spectroscopic regimes to implement the detection of gases, plasmas, liquids, and solids at a high signal-to-noise ratio level. Optical supercontinuum generation (SCG) technology is an

indispensable technique for producing supercontinuum white laser sources. The most popular routine towards SCG is harnessing the third-order optical nonlinear (3rd-NL) effects like self-phase modulation (SPM) in noncrystalline materials driven by a high peak power femtosecond pump pulse. The power density should be very high, up to tens of GW/cm² to ignite significant 3rd-NL interaction. One popular way is to concentrate the pump laser pulse energy at a tiny space region such as the core of a microstructured fiber,^{5–9} but this method has some defects, such as small modal area, low pulse energy ($\ll 1 \mu\text{J}$), low brightness, and poor spectral profile flatness. An alternative way is to use a very high-energy pump laser beam to pump bulk materials but with the optical energy diluted in a large cross section.^{10–12} However, the dispersion of bulk materials is hard to engineer up to an ideal level, so the expansion of the SCG bandwidth is well below the scheme of the microstructured fiber. Recently, a promising

*Address all correspondence to Zhi-Yuan Li, phzyli@scut.edu.cn

pathway creating a high-performance supercontinuum white laser has been explored by deeply engineering synergic second-order nonlinearity (2nd-NL) and 3rd-NL effects in a single chirped periodically poled lithium niobate (CPPLN) nonlinear crystal or cascaded optical module via ultrabroadband quasi-phase-matching (QPM) schemes in terms of much higher energy ($>100 \mu\text{J}$ per pulse), broader bandwidth, and a flatter spectral profile.^{13–17} Nonetheless, these techniques all face an inescapable challenge in accommodating more powerful input pulses due to the optical damage and laser destruction of bulk solid materials.

One way to increase the pulse energy of a supercontinuum laser to a very high level without causing optical damage is to inject a high pulse energy femtosecond laser into a long-path gas-filled hollow-core fiber (HCF).^{18,19} However, such a device encounters certain limitations in the balanced performance of spectral bandwidth, spectral flatness, and pulse energy due to the low nonlinear coefficient of the rare gas. At the same time, HCF compressors suffer several technical complications, including a sizable footprint, delicate construction, poor long-term stability, and cumbersome operation calibration. For these reasons, the natural choice to create a long-lived, high-stability, and inexpensive SCG seems to be using liquids like water.^{20,21} Liquids can withstand high enough pulse energies, effectively removing the optical damage problems commonly existing in solid materials. Yet, the SCG generated in these liquid media still faces some shortcomings, where the spectra show a strong intensity peak lying at the pump central wavelength much higher than the sidebands, and thus the overall spectral flatness is quite low due to the limitation of purely 3rd-NL in expanding the bandwidth of pump laser.^{20,21} In this work, we demonstrate an intense and flat supercontinuum spectrum covering 413 to 907 nm in a bandwidth of 10 dB and reaching a high energy of 0.6 mJ per pulse from a synergic water and CPPLN module driven by 4 mJ pulse energy and 50 fs pulse duration Ti:sapphire femtosecond laser. The secret underlying the success of this scheme lies in adopting collective 2nd-NL and 3rd-NL within the cascaded water–CPPLN module at the same time without suffering optical damage.

2 Results

2.1 Nonlinear Optical Experiments

The experimental setup is schematically shown in Fig. 1(a). The input femtosecond laser system is a Ti:sapphire chirped pulse amplification laser system (Coherent, Astrella USP) with a central wavelength of 800 nm, a pulse duration of 50 fs, and a repetition rate of 1 kHz, which provides maximum pulse energy up to 4 mJ. The power of the laser pulse can be adjusted by a tunable attenuator. The sample is a cascaded water–CPPLN module that is deliberately designed to manipulate the overall 3rd-NL and 2nd-NL to accomplish intense ultrabroadband white laser generation. The CPPLN crystal is immersed in distilled water filled within a fused silica cuvette with dimensions of $40 \text{ mm} \times 30 \text{ mm} \times 30 \text{ mm}$. Each wall of the cuvette is 1.5 mm thick, and the top surface is open. Meanwhile, the cuvette is placed on a translation platform, which can be moved to change the size of the incident beam at the central position of the cuvette.

In our experiment, the first-stage ultrabroadband laser source is created by remarkable 3rd-NL SPM processes in distilled water by focusing the input laser pulse with a lens of $f = 100 \text{ mm}$. The spot focus is located 20 mm behind the front

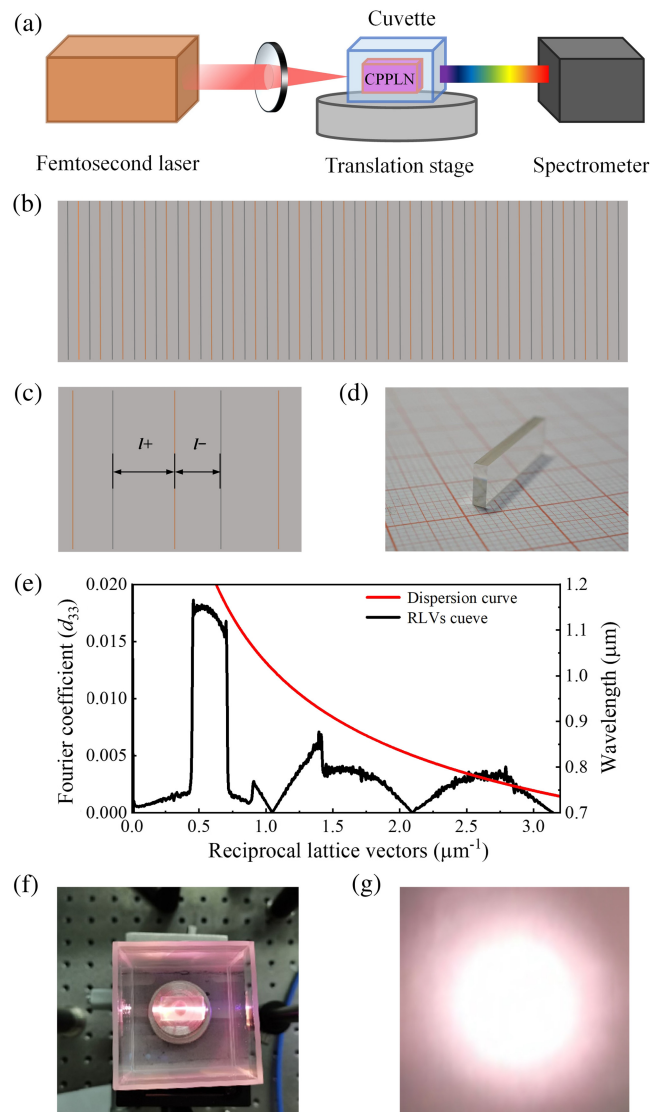


Fig. 1 (a) Nonlinear optical experimental setup. (b) Microscopic image of the fabricated sample surface of a typical CPPLN structure. (c) High-magnification view of the CPPLN sample. (d) Fabricated CPPLN sample. (e) The phase-mismatch curve for the SHG process in LN crystal combined with the Fourier-transform spectrum for CPPLN structure. (f) Photographs of the water–CPPLN module illuminated by the 800 nm Ti:sapphire laser. (g) The white-light spot emitting from the water–CPPLN module.

wall of the cuvette filled with water. Then, the generated supercontinuum emission from water is used as a driver for the continuous broadband SHG process within the CPPLN sample to further expand the shortwave segments, finally leading to the creation of a bright, ultrabroadband, and superflat supercontinuum white laser. The poling period of CPPLN is described by $\Lambda(y) = \Lambda_0/[1 + (D_g \Lambda_0 y/2\pi)]$, where Λ_0 is the starting period and D_g is the chirp date. The reciprocal vector $G_m(y)$ provided by the CPPLN structure is inversely proportional to the poling period $\Lambda(y)$, that is, $G_m(y) = 2m\pi/\Lambda(y)$, where m represents the QPM order. One can easily choose appropriate values of $\Lambda(y)$, m , and $G_m(y)$ so that QPM is satisfied. In our experiment, the poling period of CPPLN is specially designed to match with

a broadband 800 nm-centered 3rd-NL SPM broadening pump laser. The microscopic details of the fabricated sample surface are explicitly illustrated in Figs. 1(b)–1(c). The overall size of the sample is 20 mm (length) \times 6 mm (width) \times 2 mm (thickness), as displayed in Fig. 1(d). And there is no special coating on the surfaces of the CPPLN sample. We adopt an effective nonlinear coefficient model to make a qualitative QPM analysis of the designed CPPLN sample.^{22,23} The calculated Fourier-transform spectrum of the sample alongside the SHG phase-mismatching curve (versus the fundamental wavelength of 0.7 to 1.2 μm) is displayed in Fig. 1(e). The combined plots clearly show that such a designed CPPLN crystal can offer three continuous reciprocal-lattice vector bands for the direct QPM SHG against the broadband pump wavelength of 0.7 to 1.2 μm .

The output spectra are measured by a fiber-coupled spectrometer (Ocean Optics HR4000, 200 to 1100 nm). A photograph of the sample setup with a bright laser transmission channel seeded by the Ti:sapphire femtosecond laser beam at a pulse energy of 4 mJ is displayed in Fig. 1(f). As shown in Fig. 1(g), we observe a bright white-light spot with good spectral profile output from the water–CPPLN module. This naked-eye feature preliminarily shows that the output light from cascaded water–CPPLN is an ultrabroadband white laser beam that contains quite uniform visible light components.

2.2 Supercontinuum Generation in Water

To better understand the above experimental observation, we make an accurate analysis of the spectral profile and energy power along the optical path in Fig. 1(a). The setup in Fig. 1(a) can be categorized into two cascaded parts. The first part is composed of the Ti:sapphire femtosecond laser and pure water, while the second part involves the CPPLN sample. The first part relies on the 3rd-NL to create SCG, which then serves as the pump laser seeds for the second part that adopts the 2nd-NL to convert the incoming long-wavelength laser into a short-wavelength ultrabroadband SHG laser.

As a reference experiment, we first measure and analyze the supercontinuum output spectra generated in pure water without involving CPPLN and under different input pulse energies. The results are shown in Fig. 2. The supercontinuum spectra at the

pump pulse energies of 1.75, 2, 3.5, and 4 mJ are found to involve a series of visible (Vis) to near-infrared (NIR) bands covering around 633 to 890 nm, 510 to 903 nm, 487 to 905 nm, and 478 to 913 nm, respectively, counted at a -10 dB intensity level. The 10 dB bandwidths are 257, 393, 418, and 435 nm, respectively. The magnitude of spectral broadening is positively correlated with the pump pulse power density, which induces a large frequency broadening effect and creates a supercontinuum spectrum 1 order of magnitude broader than the pump femtosecond laser (~ 55 nm 10 dB bandwidth), meanwhile showing high spectral flatness. The corresponding output light signals after the water have power levels of 0.84, 0.92, 1.5, and 1.7 mJ per pulse, with the energy conversion efficiencies being 48%, 46%, 43%, and 42.5%, respectively.

It is interesting to note that the maximum peak of the expanded spectra is still located rightly at the pump laser wavelength, ~ 800 nm, in the NIR regime. This is in accordance with the popular idea that the phenomenon is a well-known supercontinuum effect originating from the 3rd-NL SPM effect. Yet, there appears a significant shoulder peak that is centered at 560 nm and ranges between 515 and 598 nm, located in the green-yellow regime. The intensity is only 7 dB lower than the main peak (namely 20% of the main peak intensity), a quite remarkable high value. The appearance of these shoulder peaks obviously goes beyond the purely SPM effect and must be understood from other physical mechanisms, which will be discussed later. Despite complicated spectral profiles observed in experiments, our results clearly indicate that the first part of the optical setup in Fig. 1(a) can create a bright, flat, and broadband SCG laser source for seeding ultrabroadband continuous SHG process within the second-part CPPLN sample. Notably, the use of water as a 3rd-NL medium can successfully avoid the optical damage problem commonly occurring in solid materials and in principle withstand a very high pump energy. In comparison, when focusing a Ti:sapphire fs laser into solid materials like silica and LN by $f = 100$ mm lens, a modest energy value of 120 μJ per pulse, which is 33 times smaller than the current 4 mJ pulse energy, is sufficiently large to cause apparent optical damage to solid materials. Thus, liquid media like water indeed can provide an economical and effective technical way for high-energy and high-stability 3rd-NL SCG.

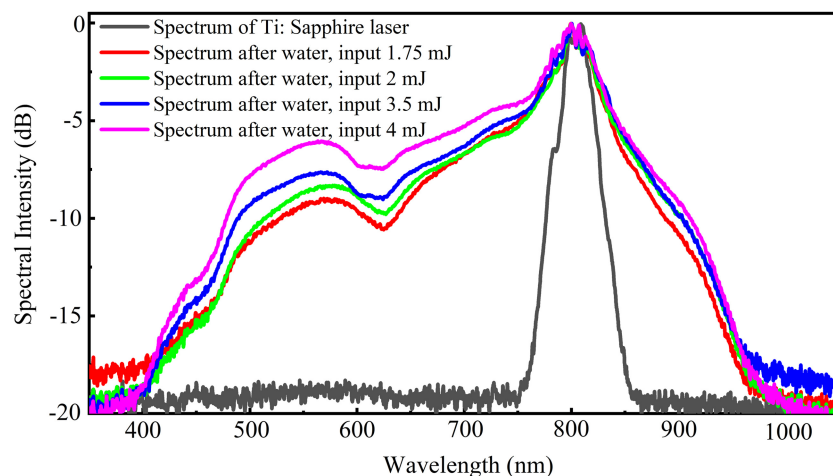


Fig. 2 Normalized supercontinuum spectra taken after water with different input pulse energies.

2.3 Supercontinuum Generation via Synergic Water–CPPLN Module

In the next step of the nonlinear experiment, the CPPLN sample is added and immersed in water. The 800 nm pump laser is focused in water, ~ 1 mm after the front surface of CPPLN, and drives the 2nd-NL SHG effect to take action. We monitor and measure the spectral evolution of supercontinuum white lasers emitting from the cascaded water–CPPLN module with different incident pulse energies and light spot diameters. The results are shown in Fig. 3. When the pump laser has a spot diameter of 1.5 mm at the CPPLN front surface, the supercontinuum spectrum generated at 4 mJ input pulse energy is significantly broader than that at the 2 mJ level, as displayed by the blue and green curves in Fig. 3. Both supercontinuum spectra exhibit one main peak and a strong shoulder peak, with the 4 mJ spectrum covering 413 to 907 nm with 494 nm 10 dB bandwidth, and the 2 mJ spectrum spanning 420 to 870 nm with 450 nm 13 dB bandwidth. In addition, the overall output pulse energies from the water–CPPLN module are 0.6 and 0.25 mJ, with the conversion efficiencies being 15% and 12.5%, respectively. The energy conversion efficiencies for the mere CPPLN crystal are 30% and 27%, respectively, at the 4 and 2 mJ pump levels. When we enlarge the diameter of the spot incident on the front face of the CPPLN crystal to 2 mm with 4 mJ pulse energy, the generated supercontinuum spectrum, in this case, is slightly narrowed and spans 417 to 903 nm with a 10 dB bandwidth of 486 nm, as indicated by magenta curve in Fig. 3. It can also be seen that the 4 mJ shoulder peak centered at 520 nm is very strong, only 10% in magnitude lower than the 800 nm main peak, indicating a very strong SHG effect takes action. When the optical intensity is reduced, the shoulder peak quickly lowers down. These results imply that the nonlinear optical responses of water–CPPLN are closely related to the peak power density of the pump pulse laser, which can be adjusted by the input laser energy or incident light spot diameter.

Obviously, an optimal supercontinuum spectrum extending from 413 to 907 nm at 10 dB bandwidth can be obtained from the cascaded water–CPPLN module in the case of 4 mJ input pulse energy and an incident spot diameter of 1.5 mm on the front end of the CPPLN crystal. The ~ 500 nm spectral

bandwidth is about 10 times that of the pump Ti:sapphire femtosecond laser (slightly below 55 nm), which is a magnificently large number of bandwidth broadening. Clearly, the intense SCG is primarily governed by both high-efficiency ultrabroadband SHG processes and SPM spectral broadening at harmonics signals within the water–CPPLN module, finally forming a more than one-octave 10 dB bandwidth covering Vis–NIR regions. The collective action of 2nd-NL and 3rd-NL effects injects new momentum into the generation of supercontinuum white lasers far exceeding any single action of them. Moreover, due to the high pump intensity and high conversion efficiency of the water–CPPLN nonlinear module, the power level of this Vis–NIR supercontinuum white laser reaches a quite high level at 0.6 mJ under the illumination of an engineered broadband pump condition that is fulfilled by delivering a 4 mJ per pulse Ti:sapphire femtosecond laser into the water to initiate a 1.7 mJ per pulse supercontinuum laser. The peak intensities of the input laser beam at the two stages are 5197 and 282 GW/cm^2 , respectively. Moreover, the water–CPPLN module can be free of damage, even in the case of a much higher pump, by adjusting the light spot size incident into the CPPLN crystal, which exquisitely controls the peak intensity of the input laser beam well below the optical damage threshold.

2.4 Nonlinear Optical Physics Analysis

To reveal the subtle physics underlying the complicated 3rd-NL broadening spectra shown in Fig. 2, we theoretically model and numerically simulate the pump pulse propagation and nonlinear interaction within water using parameters similar to our experiment and see the specific roles various physical mechanisms play. Note that within 3rd-NL, we only consider the SPM effect. We first set an initial Ti:sapphire Gaussian pulse centered at 800 nm with a pulse duration of 50 fs and pulse energies of 1.75, 2, 3, and 4 mJ to act as the seed laser pulse. In the first step, we model the 3rd-NL spectral evolution within water at different pulse energies in the framework of a simplified one-dimensional nonlinear Schrödinger equation, including the linear dispersion and SPM effects.^{24,25} The nonlinear refractive index n_2 of the water used is $1.6 \times 10^{-20} \text{ m}^2/\text{W}$. Meanwhile, we have fully considered light absorption by water, which is significant in

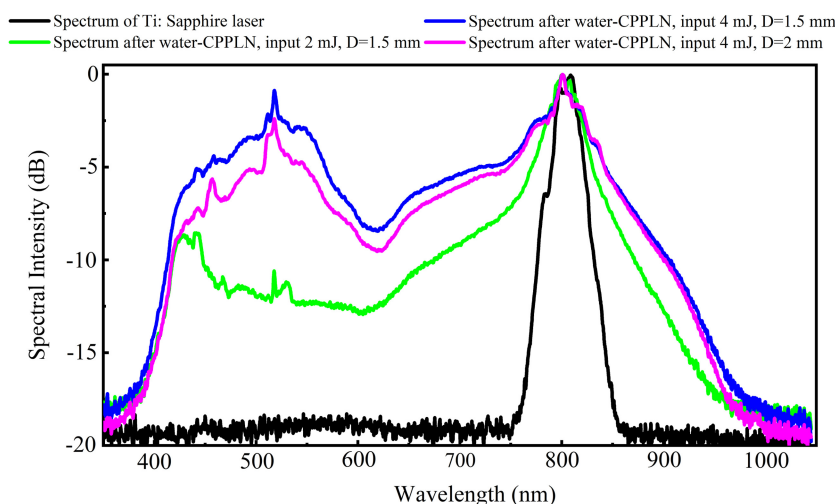


Fig. 3 Normalized supercontinuum spectra emitting from the water–CPPLN module at different input pulse energies and incident light spot diameters.

the Vis–NIR band, especially the characteristic absorption bands located at the central wavelengths of 970 and 1400 nm.^{26–28} The calculated output spectra are illustrated in Fig. 4(a). One can see that along with increasing pump energy, the spectra emitted from water show significant spectral broadening with a range of 554 to 963 nm, 542 to 963 nm, 489 to 967 nm, and 476 to 968 nm, respectively, at a bandwidth of 10 dB, which correctly captures many of the experimental features in terms of spectral broadening profile and extent. The spectra at different energies are all affected by the prominent absorption band of liquid water at 970 nm, with -20 dB attenuation in the NIR band up to 1006 nm, which is consistent with the experimental results showing a sharp drop in spectral strength above 950 nm. Meanwhile, the stronger absorption of water in the long-wave band results in a blueshifted peak wavelength, instead of being located at 800 nm,

showing the same trend as the experimental profiles (see Fig. 2). On the other hand, if the water absorption is completely neglected, we can see from the blue dotted line in Fig. 4(a) that the supercontinuum spectrum decays very slowly away from 800 nm into the infrared band, e.g., 1200 nm.

We further calculate to monitor the spectral broadening evolution along with the transport path of the pump laser within the 40 mm-length liquid water at 4 mJ pump energy. The result is shown in Fig. 4(b). One can clearly see that the spectral bandwidth increases continuously with the transmission distance. When transmitting by about 0.25 cm, the long-wave portion of the spectrum has broadened to touch the water absorption band of nearly 970 nm and starts to suffer strong NIR absorption of water. The spectral broadening reaches its maximum value covering 477 to 968 nm with 10 dB bandwidth at the 1 cm

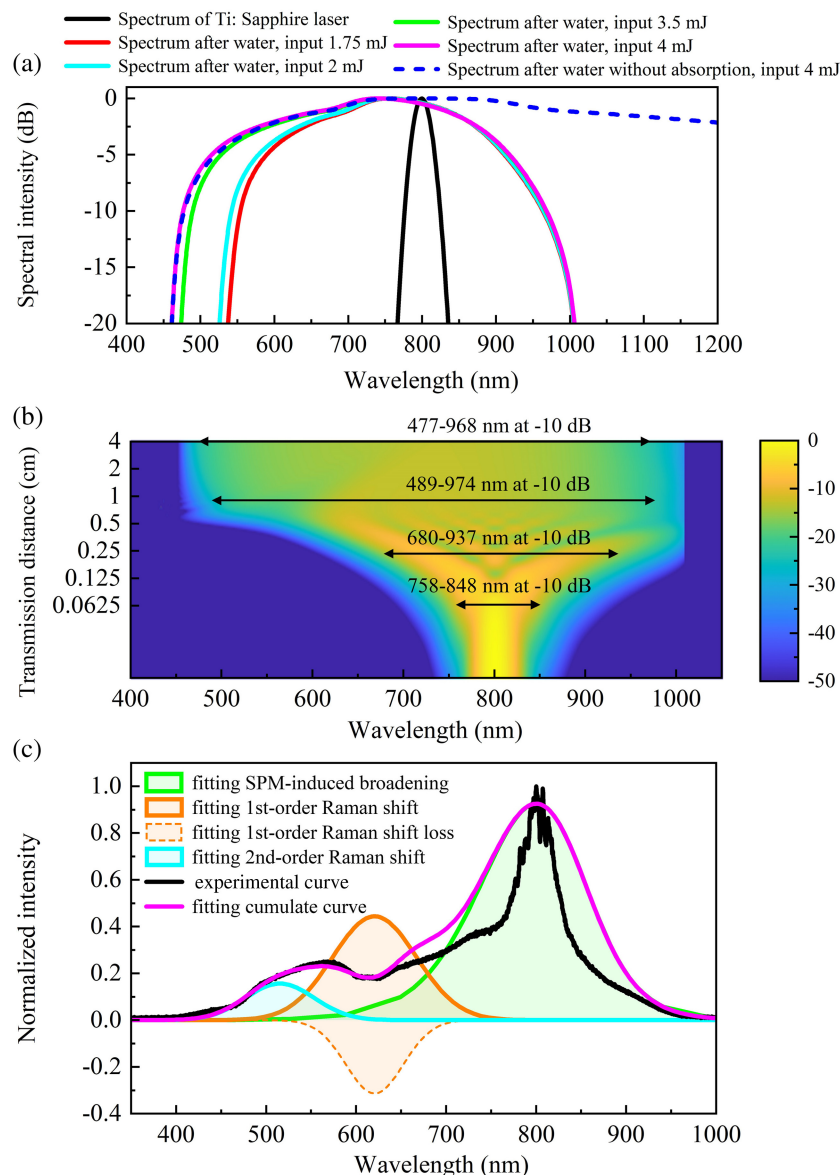


Fig. 4 (a) Simulated output spectra via SPM from water at different input energies. (b) Simulated spectral evolution at different positions within a 40 mm-length water at 4 mJ pump pulse energy. (c) Linear fitting processes modeling the supercontinuum experiment within water under the pump of 4 mJ pulse energy.

transmission distance. Overall, the SPM-induced spectral evolution calculation results provide a good description of the experimental supercontinuum spectra within the water (see Fig. 2). However, the agreement between the measured and calculated spectral profiles is not good enough. The most remarkable point is that the calculated spectra do not exhibit any shoulder peak covering 515 to 598 nm that apparently appears in the experimental measurement. We attribute this strong shoulder peak to the stimulated Raman scattering (SRS) effects of liquid water^{29,30}, which are ignored in our simulations.

We have examined more closely the nonlinear dynamics of the supercontinuum spectrum emitted from water at a 4 mJ pump by accounting for both 3rd-NL SPM and SRS effects and performing reasonable curve-fitting upon the resultant broadening supercontinuum spectrum profile. The relevant fitting results considering different nonlinear processes are shown in Fig. 4(c). Here, the generated supercontinuum signal (the black line in Fig. 4) is seen to undergo three active processes involving the SPM effect centered at 800 nm, first-order, and second-order SRS effects. If only considering the mere 3rd-NL SPM effect, the resulting spectrum will simply be a narrow band curve covering about 651 to 922 nm (10 dB bandwidth), as displayed by the green curve in Fig. 4, without showing any shoulder peak. Notice water exhibits a series of Raman peaks covering 3074 to 3666 cm^{-1} ,²⁹ and the first-order SRS under pumping by 800 nm would yield a shoulder peak at 621 to 642 nm. The obtained typical first-order Raman spectrum of water is illustrated by the orange solid curve in Fig. 4(c). The second-order SRS would be immediately excited due to such a strong laser pumping condition. This process can be assumed as another first-order SRS-induced loss (depicted by the dotted line inverse peak) to the secondary spectral peak centered at 621 nm [the orange dotted curve in Fig. 4(c)] and transfer of energy to a minor shoulder peak in the range of 507 to 586 nm [as seen in the azure curve of Fig. 4(c)]. Then, we fit linearly the above three nonlinear optical interactions individually and finally acquire the magenta cumulate curve in Fig. 4(c). One can clearly see that the final fitted curve presents a good consistency with the experimental result. These analyses clearly indicate that under the pump by a large-energy 800 nm Ti:sapphire femtosecond pulse laser, the SCG within water strongly relies on the collective and simultaneous actions of 3rd-NL SPM and SRS effects, as well as the linear light absorption effect of water. Such abundant nonlinear dynamic processes within water provide more freedom for the generation of a better supercontinuum white laser with elevated spectral profile performance in terms of spectral bandwidth and flatness, which then serve as a more ideal seed for driving the ultrabroadband SHG process in the second-part CPPLN structure.

Now we return to the experimental spectral profile seen in Fig. 3 for the water–CPPLN module, which exhibits a very prominent shoulder peak spanning 450 to 600 nm at the 4 mJ pump energy. We believe that the second-order SRS of water, forming the shoulder peak in Fig. 2, will still make a considerable contribution. Yet, this spectral strength is negligible at around 400 nm. Another major contribution should come from the primary SHG of CPPLN, where both the effective nonlinear coefficient and the pump light intensity act and compete to shape the transfer behavior of the optical energy in the NIR band to the Vis band. What is the pump light spectral intensity upon the CPPLN? Because the input 800 pump laser is focused at the front surface of CPPLN, the most prominent part of SCG

directly goes into the CPPLN without suffering much linear absorption of water. Then the spectral intensity of the secondary pump light driving the SHG should be described by the blue dotted curve in Fig. 4(a) instead of other curves suffering big infrared absorption of water. This means that up to 1200 nm, the secondary pump light spectral intensity still maintains 50% of the 800 nm peak intensity; thus the SHG is still strong up to 600 nm. On the other hand, it can be seen from Fig. 1(e) that the effective nonlinear coefficient is much smaller in the short-wavelength regime (around 700 to 900 nm) than the long-wavelength regime (around 900 to 1200 nm), the SHG intensity below 450 nm is much weaker than between 450 to 600 nm. In addition, in our experiment, we observed an obvious transport path of the white laser beam in water and ascribed this to the considerable Rayleigh scattering of the white laser by tiny air bubbles induced by infrared light absorption by water and consequent heating to water. Such a Rayleigh scattering is much larger in blue and violet bands than the green-yellow band, leading to great attenuation of the violet-blue band light seen in Fig. 3; therefore, the spectral intensity around 400 nm is much weaker compared with the prominent shoulder peak at 450 to 600 nm.

3 Conclusion

In summary, we have presented a simple, robust, and scalable cascaded architecture composed of water and CPPLN for generating an intense supercontinuum white laser spanning 413 to 907 nm (10 dB bandwidth) at a level of 0.6 mJ per pulse via synergic 2nd-NL and 3rd-NL effects. Utilizing water as a 3rd-NL SPM spectral broadening medium instead of usual solid media provides a defined path for scaling the pump energy of a Ti:sapphire femtosecond laser, even up to the 4 mJ regime, simultaneously effectively avoiding optical damage. In addition, water exhibits very prominent first-order and second-order SRS effects, inducing considerable shoulder peaks in the short-wavelength regime in both pure water and the cascaded water–CPPLN modules. This water–CPPLN scheme enables a new technological path to be explored with a long-lived, high-stability, and inexpensive “three high” white laser in terms of intense pulse energy, high spectral flatness, and ultrabroad bandwidth. We anticipate that this robust ultrabroadband supercontinuum source will enable new modalities in ultrafast spectroscopy and hyperspectral imaging, as well as opportunities to resolve ultrafast dynamics of multiple physical, chemical, and biological processes over extreme spectral bandwidths with a high signal-to-noise ratio.

Disclosures

The authors declare no competing financial interests.

Code and Data Availability

The data that support the findings of this study are available from the corresponding author upon reasonable request.

Acknowledgements

This work was supported by the Science and Technology Project of Guangdong (Grant No. 2020B010190001), the National Natural Science Foundation of China (Grant No. 11974119), the Guangdong Innovative and Entrepreneurial Research Team Program (Grant No. 2016ZT06C594), and the National Key R&D Program of China (Grant No. 2018YFA 0306200).

References

- J. Fan et al., “Video-rate imaging of biological dynamics at centimetre scale and micrometre resolution,” *Nat. Photonics* **13**, 809 (2019).
- Y. Nakano, T. Imasaka, and T. Imasaka, “Generation of a nearly monocycle optical pulse in the near-infrared region and its use as an ionization source in mass spectrometry,” *Anal. Chem.* **92**, 7130 (2020).
- S. V. Smirnov et al., “Optical spectral broadening and supercontinuum generation in telecom applications,” *Opt. Fiber Technol.* **12**, 122 (2006).
- A. Dubietis, A. Couairon, and G. Genty, “Supercontinuum generation: introduction,” *J. Opt. Soc. Am. B* **36**, SG1 (2019).
- P. Russell, “Photonic crystal fibers,” *Science* **299**, 358 (2003).
- X. Jiang et al., “Deep-ultraviolet to mid-infrared supercontinuum generated in solid-core ZBLAN photonic crystal fibre,” *Nat. Photonics* **9**, 133 (2015).
- J. K. Ranka, R. S. Windeler, and A. J. Stentz, “Optical properties of high-delta air-silica microstructure optical fibers,” *Opt. Lett.* **25**, 796 (2000).
- T. L. Cheng et al., “Mid-infrared supercontinuum generation spanning 2.0 to 15.1 μm in a chalcogenide step-index fiber,” *Opt. Lett.* **41**, 2117 (2016).
- F. Belli et al., “Vacuum-ultraviolet to infrared supercontinuum in hydrogen-filled photonic crystal fiber,” *Optica* **2**, 292 (2015).
- V. Shumakova et al., “Multimillijoule few-cycle mid-infrared pulses through nonlinear self-compression in bulk,” *Nat. Commun.* **7**, 12877 (2016).
- F. Silva et al., “Multi-octave supercontinuum generation from mid-infrared filamentation in a bulk crystal,” *Nat. Commun.* **3**, 807 (2012).
- P. He et al., “High-efficiency supercontinuum generation in solid thin plates at 0.1 TW level,” *Opt. Lett.* **42**, 474 (2017).
- B. Q. Chen et al., “White laser realized via synergic second- and third-order nonlinearities,” *Research* **2021**, 1539730 (2021).
- M. Z. Li, L. H. Hong, and Z. Y. Li, “Intense two-octave ultraviolet-visible-infrared supercontinuum laser via high-efficiency one-octave second-harmonic generation,” *Research* **2022**, 9871729 (2022).
- L. Hong et al., “350-2500 nm supercontinuum white laser enabled by synergic high-harmonic generation and self-phase modulation,” *Photonix* **4**, 11 (2023).
- L. Hong et al., “Intense ultraviolet-visible-infrared full-spectrum laser,” *Light Sci. Appl.* **12**, 199 (2023).
- L. Hong et al., “Intense and superflat white laser with 700 nm 3 dB bandwidth and 1 mJ pulse energy enabling single-shot femtosecond-pulse-laser spectroscopy,” *Research* **6**, 0210 (2023).
- M. T. Hassan et al., “Optical attosecond pulses and tracking the nonlinear response of bound electrons,” *Nature* **530**, 66 (2016).
- S. Fang et al., “Generation of sub-900- μJ supercontinuum with a two-octave bandwidth based on induced phase modulation in argon-filled hollow fiber,” *IEEE Photonics Technol. Lett.* **23**, 688 (2011).
- T. Jimbo et al., “Enhancement of ultrafast supercontinuum generation in water by the addition of Zn^{2+} and K^{+} cations,” *Opt. Lett.* **12**, 477 (1987).
- C. Wang et al., “Femtosecond filamentation and supercontinuum generation in silver-nanoparticle-doped water,” *Appl. Phys. Lett.* **90**, 181119 (2007).
- M. L. Ren and Z. Y. Li, “An effective susceptibility model for exact solution of second harmonic generation in general quasi-phase-matched structures,” *Europhys. Lett.* **94**, 44003 (2011).
- C. Y. Hu and Z. Y. Li, “An effective nonlinear susceptibility model for general three-wave mixing in quasi-phase-matching structure,” *J. Appl. Phys.*, **121**, 123110 (2017).
- J. M. Dudley, G. Genty, and S. Coen, “Supercontinuum generation in photonic crystal fiber,” *Rev. Mod. Phys.* **78**, 1135 (2006).
- M. Bache, J. Moses, and F. W. Wise, “Scaling laws for soliton pulse compression by cascaded quadratic nonlinearities,” *J. Opt. Soc. Am. B* **24**, 2752 (2007).
- B. Wozniak and J. Dera, *Light Absorption in Sea Water*, Springer, New York, (2007).
- G. M. Hale and M. R. Querry, “Optical constants of water in the 200 nm to 200 μm wavelength region,” *Appl. Opt.* **12**, 557 (1973).
- R. A. J. Litjens, T. I. Quickenden, and C. G. Freeman, “Visible and near-ultraviolet absorption spectrum of liquid water,” *Appl. Opt.* **38**, 1216 (1999).
- S. M. Baschenko and L. S. Marchenko, “On Raman spectra of water, its structure and dependence on temperature,” *Semicond. Phys. Quantum* **14**, 77 (2011).
- F. Perakis et al., “Vibrational spectroscopy and dynamics of water,” *Chem. Rev.* **116**, 7590 (2016).

Lihong Hong received her BS degree in optical information science and technology from Fujian Normal University in 2016, her MS degree in optics from South China University of Technology in 2019 under the supervision of professor Zhi-Yuan Li, and her PhD in physics from South China University of Technology in 2023 under the supervision of professor Zhi-Yuan Li. She is now a postdoctoral fellow of the State Key Laboratory of High Field Laser Physics, Shanghai Institute of Optics and Fine Mechanics, Chinese Academy of Sciences; her co-supervisors are academician Ruxin Li and professor Zhi-Yuan Li. Her research interests cover the theory and experiment of nonlinear and ultrafast optics and laser technology.

Yuanyuan Liu received her BS degree in the School of Physics and Optoelectronics from South China University of Technology in 2021. She is now a PhD student in physics at South China University of Technology under the supervision of professor Zhi-Yuan Li. Her research interests cover the theory and experiment of nonlinear and ultrafast optics and laser technology.

Yujie Peng is a professor at Shanghai Institute of Optics and Fine Mechanics, Chinese Academy of Sciences. He is committed to the research of ultra-intense and ultra-fast lasers, especially for the high power lasers, mid-infrared ultra-fast lasers, and so on. He was also participated in the construction of several ultra-intense laser facilities, such as Shanghai super-intense ultra-fast laser facility (SULF) and SHINE-SEL facility.

Ruxin Li is a professor at Shanghai Institute of Optics and Fine Mechanics, Chinese Academy of Sciences. He is committed to the research of ultra-intense and ultra-fast lasers. He was elected as the OSA Fellow in 2014 and elected as the academician of Chinese Academy of Sciences in 2017. He is the vice chairman of the Chinese Optical Society and he was the chairman of the Asian Intense Laser Network during 2010 to 2014. He is the committee member of the International Committee on Ultra-Intense Lasers (ICUIL).

Zhi-Yuan Li received his BS degree in optoelectronics from the University of Science and Technology of China, Hefei, in 1994 and his PhD in optics from the Institute of Physics, Chinese Academy of Sciences, Beijing, in 1999, where he served as a principal investigator from 2004 to 2016. He is now a professor and associate dean of the School of Physics and Optoelectronics at the South China University of Technology, Guangzhou. His research interests cover the theory and experiment of photonic crystals, metamaterials, plasmonics, nonlinear and ultrafast optics, laser technology, quantum optics, quantum physics, and optical tweezers.

Biographies of the other authors are not available.